Discover Civil Engineering

Research

A numerical study on effect of liquefaction on ring footings during 2001 Bhuj earthquake at Kutch (Gujarat), India

Milind Amin[1] · Manendra Singh[2]

Abstract

Liquefaction, the temporary loss of strength in saturated sand causing it to behave like a liquid, leads to devastating consequences, including the settling, tilting, or collapsing of structures built on loose, saturated soil. The 2001 Bhuj earthquake witnessed extensive liquefaction in regions such as the Great Rann of Kutch, Banni Plains, Kandla, and Gulf of Kutch, resulting in substantial damage to various infrastructures, including bridges, docks, buildings, embankments, and dams. This study employs a finite element approach to analyse the behaviour of shallow foundations on liquefying subsoil in Kutch during the 2001 earthquake. The investigation focuses on ring footings with inner radii of 0.25 m, 0.5 m, and 0.75 m, as well as an outer radius of 1 m, alongside a circular foundation with a 1 m radius. Notably, the ring footing with a radius ratio of 0.5 exhibits the least settlement under static loads, underscoring that liquefaction-induced settlement for ring footings is significantly less than that for circular footings.

Abbreviations

FE	Finite element
Υ	Unit weight
IS	Indian standard
Mw	Earthquake moment magnitude
N	SPT value
P_A	Reference stress
R_f	Failure ratio
R_i	Inner radius
R_o	Outer radius
SPT	Standard penetration test
Su	Undrained shear strength
UBC3D-PLM	University of British Columbia 3D plaxis liquefaction model
c'	Effective cohesion
fac_{dens}	Fitting parameter to adjust densification rule
fac_{post}	Fitting parameter to adjust post liquefaction behaviour
k^e_B	Elastic bulk modulus number

✉ Manendra Singh, manendra@nith.ac.in; Milind Amin, 102114001@smail.iitpkd.ac.in | [1]Department of Civil Engineering, Indian Institute of Technology, Palakkad, Kerala 678623, India. [2]Department of Civil Engineering, National Institute of Technology, Hamirpur, Himachal Pradesh 177005, India.

Discover

k^e_G	Elastic shear modulus number
k^p_G	Plastic bulk modulus number
m_e	Power for stress dependency of elastic bulk modulus
n_e	Power for stress dependency of elastic shear modulus
n_p	Power for stress dependency of plastic shear modulus
φ'	Angle of internal friction
N	Ring radius ratio
PGA	Peak ground acceleration
[c]	Damping matrix
α and β	Rayleigh damping coefficients
Φ_{mob}	Mobilised friction angle
φ'_{cv}	Friction angle at constant volume
φ'_p	Peak friction angle
ψ	Angle of dilatancy
$(N_1)_{60}$	Corrected SPT blow counts
σ'_v	Vertical effective stress after dynamic analysis
σ'_{v0}	Initial effective stress before seismic activity
z	Depth
[M]	Mass matrix
[K]	Stiffness matrix

1 Introduction

In recent advancements, Onshore and offshore axisymmetric structures, like transmission towers and offshore wind turbines, often rely on ring foundations for support [12, 32]. These structures, which are typically taller than their base width, endure significant moments, horizontal forces, and vertical loads throughout their operational lifespan. Given the prevalent use of ring foundations for such structures, understanding their behaviour under combined loading becomes imperative. While numerous studies have extensively investigated the behaviour of ring foundations under individual static loading conditions through numerical [4, 21], analytical [5, 22], and experimental studies [7, 22], their response under combined loading remains comparably less explored, unlike circular and square footings especially under seismic loading condition.

Seismicity has often played a critical role in the construction of structures and intended safety of structures, as it poses numerous risks to the structure itself, its foundation, and neighbouring infrastructures. Throughout history, earthquakes have exerted a profound influence on the areas where such phenomena occurred around the world. When shear waves are generated and propagate through various layers of soil, it can trigger soil liquefaction, jeopardising the durability and strength of numerous civil structures and posing a significant threat to human safety. Earthquake-induced liquefaction has led to catastrophic destruction globally. Notable examples include the 1964 Niigata Earthquake, 1971 Lower San Fernando Dam incident, 1979 Imperial Valley Earthquake, 1983 Nerleck Berm event, 1995 Kobe Earthquake, 1999 Chi-Chi earthquake, 2001 Bhuj Earthquake, and 2011 Christchurch Earthquake [28, 29, 37].

Various methods, including research lab experiments, in-situ tests, and model experiments, can be employed to assess the dynamic response of soil. Common laboratory tests for measuring dynamic soil properties encompass the resonant column test, cyclic triaxial test, and cyclic simple shear test [29] and [37]. In-situ tests include the Standard Penetration Test (SPT), seismic reflection test, and other seismic tests. Model test experiments involve shaking tables and centrifuge tests [26]. Additionally, several software programs are now available to predict soil behaviour during earthquakes efficiently, facilitated by advancements in computer technology [28]. Various constitutive models, such as FINN [15], BOUNDING SURFACE (1990), HYPOPLASTICITY (1994), UBCSAND (1995), PDMY02 (2003), PM4SAND (2004), NORSAND (2005), NTUA-SAND (2010), and UBC3D-PLM (2013) models, have been introduced by researchers to determine sand liquefaction behaviour.

Numerical models are essential not only for characterising the mechanical response of soil but also for conducting numerical estimations using the Finite Element approach. Advancements in constitutive models aid in analysing complex liquefaction scenarios involving intricate ground, drainage, and loading conditions [23]. For instance, the liquefaction behaviour of a homogeneous sand layer with three distinct relative densities under eleven distinct strong ground

shakings was simulated using the PM4Sand model in Plaxis-2D software [9]. Waheed and Moutaz [36] developed a numerical model of a shallow foundation using PLAXIS 3D software and validated it with past experimental results. Numerical modelling by Hong et al. [14] analysed foundation rotation due to liquefaction, revealing a significant increase in maximum and residual foundation rotation with maximal ground acceleration. Computational simulation studies conducted by Onur et al. [30] calculated the seismic influence on deformation for the Turkish city of Eskisehir, highlighting that effective pressure may rapidly equal zero in the presence of silty sands with low plasticity, leading to significant settling. Although computational analyses of liquefaction-induced settlement under buildings are abundant in the literature, only a few have addressed such issues in free-field contexts [27, 34] and [8].

The response of ring foundations in cohesionless soil during earthquakes has been analysed through FE analysis by [6]. However, this analysis primarily focused on seismic responses and did not address liquefaction scenarios. The main objective of the current study is to assess the impact of liquefaction on ring foundations situated on the Kandla, Kutch soil deposit following the Bhuj 2001 earthquake. Isolated ring footings with varying inner radii of 0.25 m, 0.5 m, and 0.75 m, all with a constant outer radius of 1 m, are utilised in the analysis. Additionally, a single circular footing with a 1 m radius and a free-field condition is included in the study. For this research, the Finite Element-based UBCSAND-PLM constitutive model is adopted, and PLAXIS 3D software is utilised for the analysis.

1.1 Site selection and soil condition

Kandla, situated in the Kutch region of Gujarat state, India, (see Fig. 1) was chosen for investigation due to the abundance of available data. Gujarat, located on the country's western coast along the Arabian Sea, is home to India's largest seaport, Kandla, within its Kutch District, near Gandhidham along the Gulf of Kutch. Much of the Gulf of Kutch consists of marshland with completely saturated soil, making it susceptible to liquefaction. The epicenter of the 2001 Bhuj earthquake is approximately 50 km away from Kandla. The soil in this area predominantly consists of fine to medium sand, with a notable presence of non-plastic particles that are highly susceptible to liquefaction during earthquakes. Table 1 provides index property data for the site. An analysis of the soil deposit at Kandla's harbour was conducted by Dash et al. [11], revealing the sensitivity of the top clay layer, which could lead to collapse during an earthquake. Notably, Dash et al. [11] reported similarities between the soil characteristics at Kandla and those observed by Sitharam and Govindaraju [33]. The soil profile's depth is depicted in Fig. 2, and for this study, the groundwater table was assumed to be at a depth of 2.50 m below the surface.
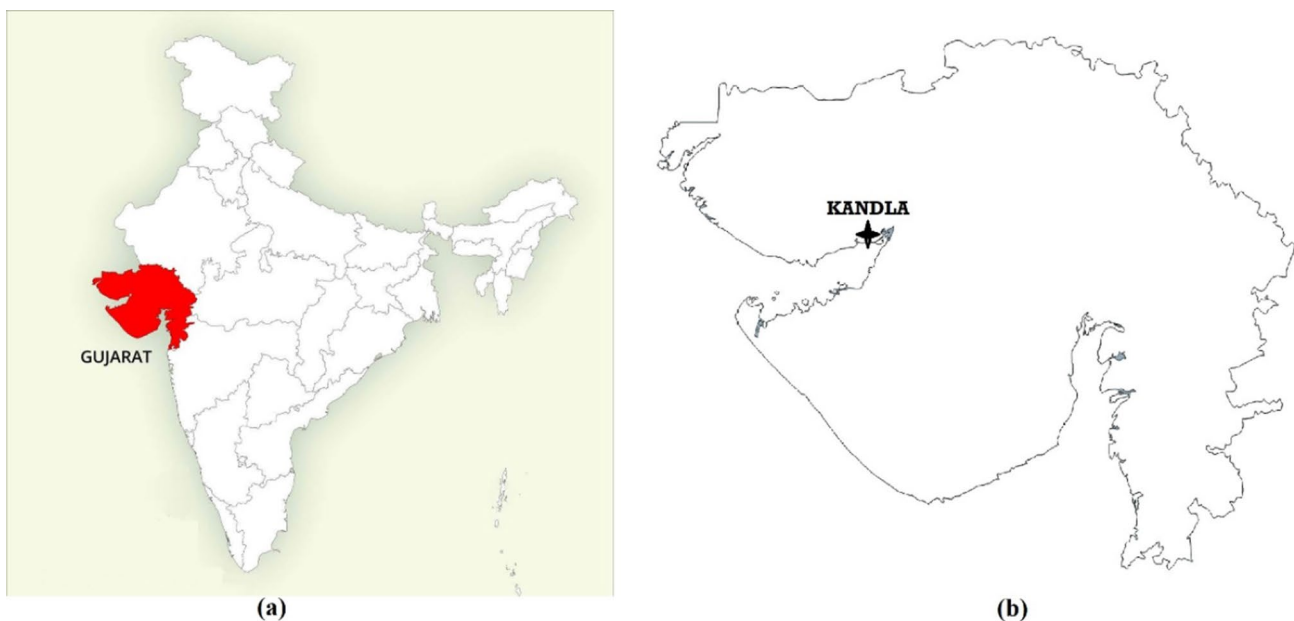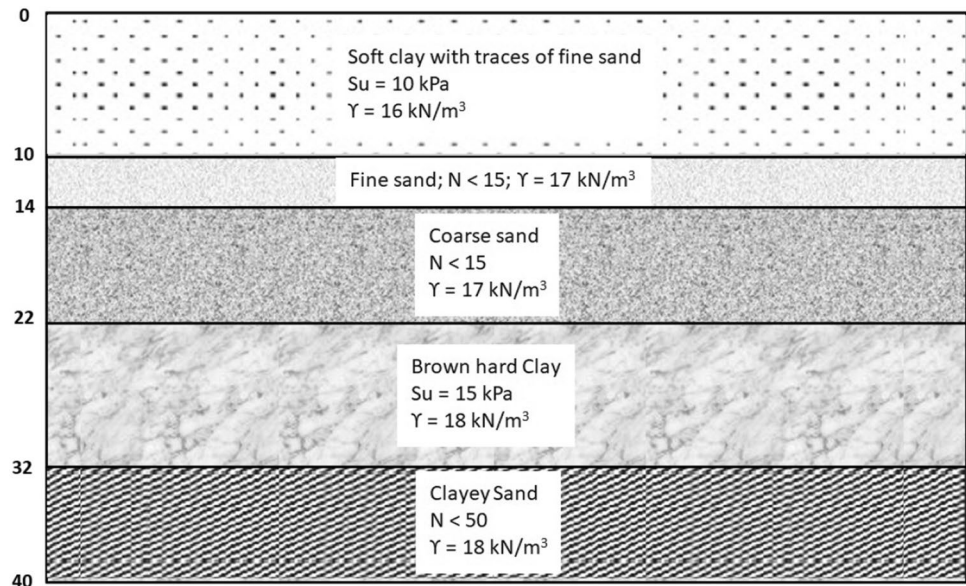

Fig. 1 Site on Geographical map **a** Location Gujarat in India; **b** Location of Kandla in Gujarat

Table 1 Bhuj sand characteristics [33]

Properties	Value
Specific gravity	2.66
Coarse sand (%)	1.00
Medium sand (%)	39.42
Fine Sand (%)	44.44
Silt (%)	13.00
Clay (%)	2.14
Maximum void ratio (e_{max})	0.71
Minimum void ratio (e_{min})	0.37

**Fig. 2** Soil profile layering at the Kandla Port [11]

1.2 Foundation selection

Ring footings, as opposed to circular footings, offer potential advantages in terms of efficiency and cost-effectiveness. These two types of footings differ in how stress is distributed beneath the foundation and how the footing reacts to loads. Ring footings are commonly utilised for various structures, including bridges, towers, silos, overhead water tanks, chimneys, and water tanks, due to its ability to maximise the potential of soil and reduce tension beneath the foundation. It is particularly beneficial for structures subject to structural stress and lateral wind-induced loads. Figure 3 provides a schematic representation of the ring footings used in this study.

1.3 The selection of earthquake motion

The Kutch region has experienced several significant earthquake events over the years, with dates detailed in Table 2, attesting to its high seismic activity. After the 2001 Bhuj earthquake, the Bureau of Indian Standards updated India's seismic zoning in 2002 [17]. According to the revised mapping, the modern Kutch district in Gujarat falls within seismic zone V, as indicated in Fig. 4. This entire highlighted area within seismic zone V encompasses the Kutch district.

    On January 26, 2001, a devastating earthquake with a magnitude of 7.7 (Mw 7.7) struck Gujarat, India. The earthquake's epicenter was located 23.6 km beneath the surface, at latitudes 23.36°N and longitudes 70.34°E. It occurred on the Kutch Mainland Fault, approximately 70 km northeast of Bhuj city, near Bachau. This event, known as the Bhuj Earthquake, stands as one of India's most catastrophic disasters. The Kutch area, situated north of the Kutch Mainland Fault, includes the Banni Plains and the Rann of Kutch. During the earthquake, strong shaking induced liquefaction
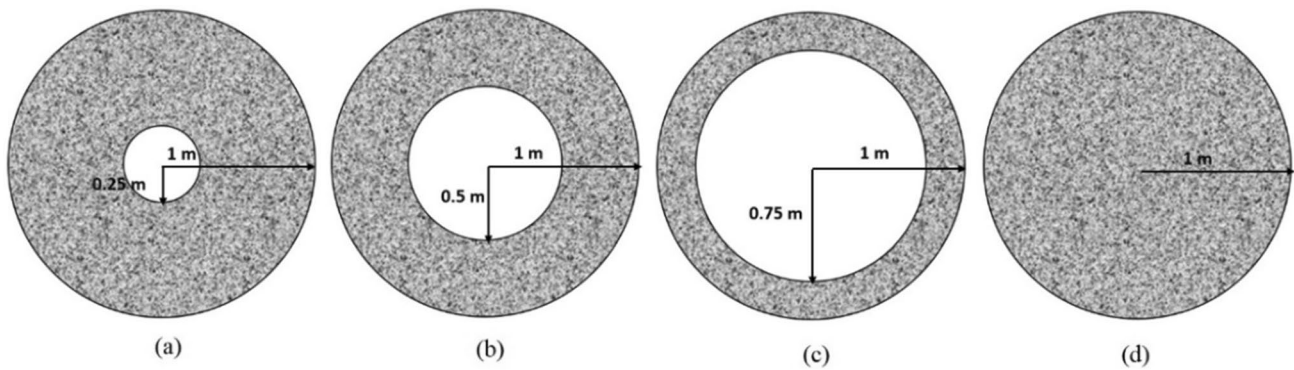
Fig. 3 **a** Ring footing having inner radius 0.25 m and outer radius 1 m; **b** Ring footing having inner radius 0.5 m and outer radius 1 m; **c** Ring footing having inner radius 0.75 m and outer radius 1 m; and **d** Circular footing having radius 1 m

Table 2 Seismic events occurred in Kutch district of Gujarat	Event	Magnitude	Name/Location
	16 June 1819	7.7–8.2	Rann of Kutch earthquake
	21 July 1956	6.1	Anjar earthquake
	26 January 2001	7.7	Bhuj earthquake
	8 April 2007	4.2	Gandhidham (Gujarat)
	18 November 2019	4.3	Bhachau in Kutch district
	5 July 2020	4.2	Bhachau in Kutch district

in the fine silts and sandy soil below the water table in the Rann of Kachchh. Consequently, the interstitial water on the surface was released, causing mineral grains to settle and significant liquefaction in some areas. This led to damage to houses, reservoirs, ports, roads, infrastructure, pipelines, and even dams, with Chang Dam and Shivlakha Dam, both located within 150 km of the epicenter, suffering significant damage.

2 Numerical modelling

2.1 Soil and foundation model

In both static and dynamic analyses, the soil model played a pivotal role. The Mohr–Coulomb model was employed for static analysis. For dynamic analysis, soil was characterised using the UBC3D-PLM sand model. The UBC3D-PLM sand model in the PLAXIS is a model used for liquefaction analysis. Development of excess pore pressure can be evaluated using UBC 3D-PLM Model whereas Mohr Columb model cannot capture the development of excess pore pressure. It is an elasto-plastic effective stress model initially introduced by Puebla et al. [31] and Beaty and Byrne [1] to model the liquefaction behaviour of sandy or silty sandy soils. UBC3D-PLM considers the Mohr–Coulomb flow condition in a three-dimensional (3D) principal stress space [31].

The material information from the Kandla site profile for the Mohr–Coulomb model is shown in Table 3. The parameters of the UBC3D-PLM model are listed in Table 4, which includes its respective units, concise explanations, and values for sand layers. Although some model parameters might lack clear physical meaning, Eqs. 1, 2, 3 and 4 were utilised to calculate these parameters, relying on correlations mentioned in [2], and used by [25].

$$k_G^{*e} = 21.7 \times 20 \times (N_1)_{60}^{0.3333} \tag{1}$$

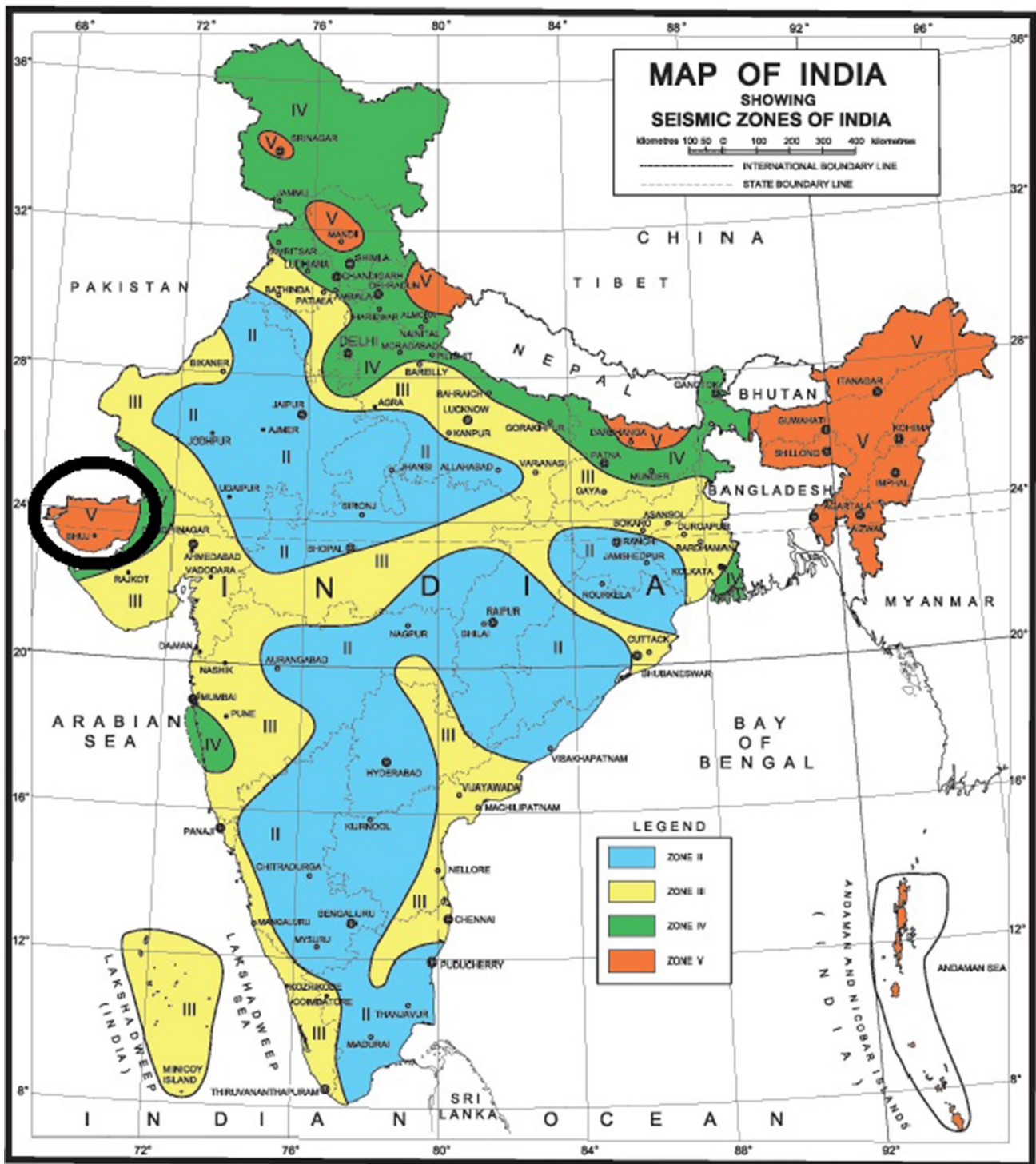$$k_B^{*e} = 0.7 \times k_G^{*e} \tag{2}$$

Fig. 4 India's seismic zone map, released by the Bureau of Indian Standards [17]

$$k_G^{*p} = k_G^{*e} \times (N_1)_{60}^2 \times 0.003 + 100 \tag{3}$$

The constant volume friction angle φ'_{cv} was determined directly from the SPT test using curves from the BIS code [18], as expressed in Eq. 4:

Table 3 Calibrated Mohr–Coulomb properties of soil layers used in the model [13]

Parameter	Unit	Soil layer				
		Soft clay	Fine sand	Coarse sand	hard clay	Clayey sand
Thickness	m	0–10	10–14	14–22	22–32	32–40
Specific weight	kN/m^3	16	17	17	18	18
Young modulus	kN/m^2	4800	4200	4800	19200	10800
Poisson's ratio	–	0.3	0.3	0.3	0.3	0.3
c'	kN/m^2	10	0	0	100	0
ϕ'	°	0	29	30	0	35
ψ	°	0	0	0	0	5

Table 4 Summarises of the parameters of the UBC3D-PLM model [35]

Parameter	Unit	Description	Fine sand layer	Coarse sand layer
		Drainage type	Undrained	Undrained
φ'_p	°	Peak friction angle	29.58	30.6
φ'_{cv}	°	Friction angle at constant volume	29	30
c'	°	Effective cohesion	0	0
k^e_B	–	Elastic bulk modulus number	546.6	552.0
k^e_G	–	Elastic shear modulus number	780.8	788.6
k^p_G	–	Plastic bulk modulus number	179.4	185.2
n_e	–	Power for stress dependency of elastic shear modulus	0.5	0.5
m_e	–	Power for stress dependency of elastic bulk modulus	0.5	0.5
n_p	–	Power for stress dependency of plastic shear modulus	0.4	0.4
R_f	–	Failure ratio	0.8445	0.8407
P_A	kN/m^2	Reference stress	100	100
fac_{dens}	–	Fitting parameter to adjust densification rule	1	1
fac_{post}	–	Fitting parameter to adjust post liquefaction behaviour	1	1
$(N_1)_{60}$	–	Corrected SPT blow counts	5	6

$$\varphi_p = \varphi_{cv} + \frac{(N_1)_{60}}{10} + \max\left(0; \frac{(N_1)_{60} - 15}{5}\right) \tag{4}$$

Combining the soil and foundation models allowed for a comprehensive analysis of the structural response to seismic forces, as discussed in the subsequent sections.

The footing data used for the analysis are presented in Table 5. The footings were constructed using Reinforced Cement Concrete (RCC) of M25 grade, with the RCC's characteristics obtained from [16]

2.2 Boundary condition

The adoption of boundary conditions is a crucial aspect of dynamic analysis, allowing the model's boundaries to condense the infinite space into a quantifiable one. For static analysis, the basic boundary was employed. In nonlinear dynamic analysis, a compliant base [20] was used at the bottom, and viscous boundary conditions [24] were applied to the side borders.

2.3 Earthquake application and damping simulation

Considering the seismic activity in the Kutch region, earthquake application and damping simulation are pivotal components of the analysis. The Kutch region had witnessed significant earthquake events over the years. However, in 2001, the availability of seismic equipment was limited. The Strong Ground Motion measuring station in the Katrol Hills proved ineffective during the earthquake. The only other reliable motion measurement instrument was installed on the first floor
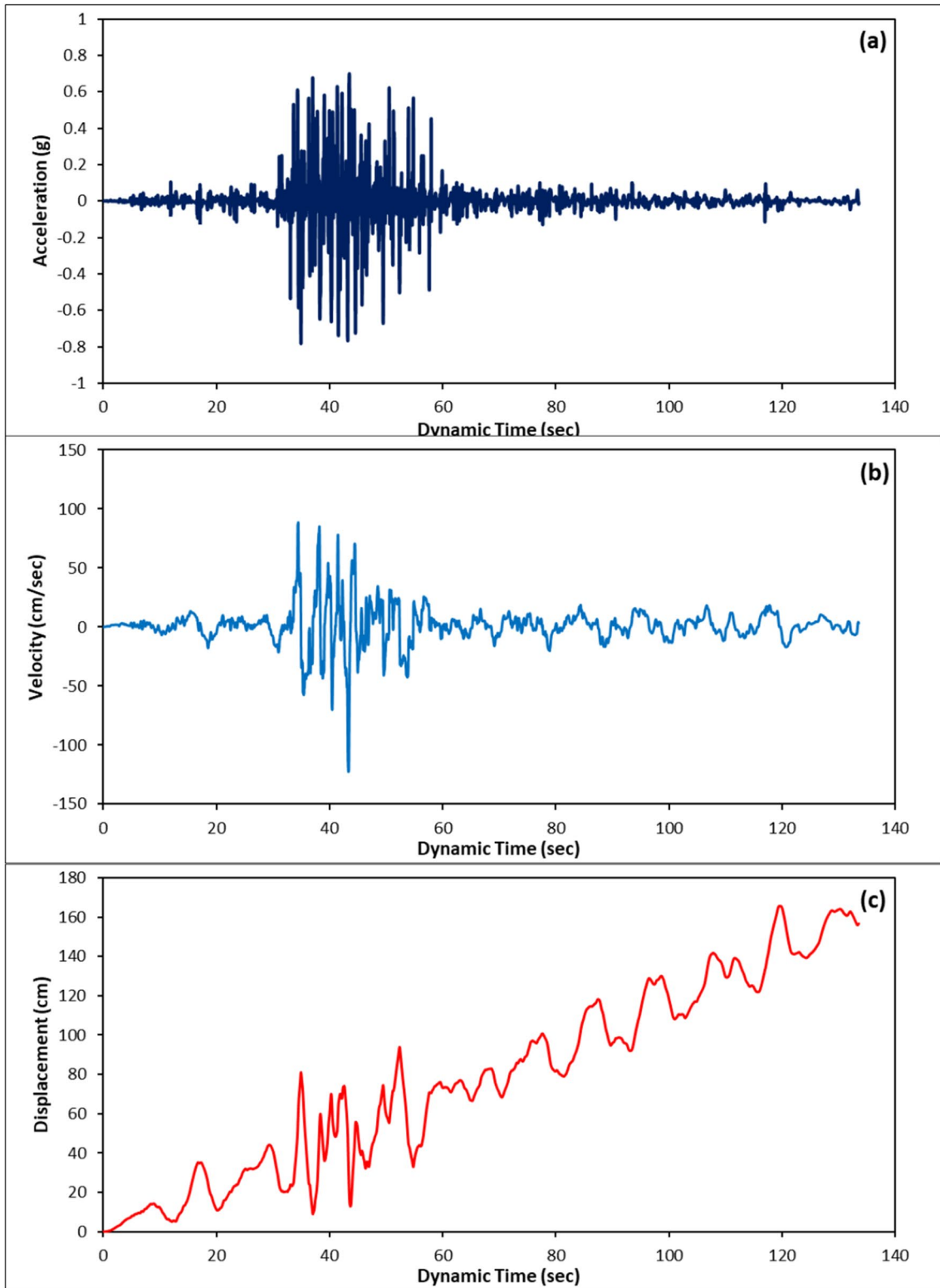
Fig. 5 Earthquake time history of Bhuj 2001 Earthquake, illustrating: **a** Acceleration; **b** Velocity; and **c** Displacement (COSMOS Strong-Motion Program Board [10])

of the Passport Office building in Ahmedabad by the University of Roorkee. Iyengar and Kanth [19] examined the Strong Ground Motion of the Bhuj earthquake, suggesting a PGA in Bhuj ranging from 0.31 g to 0.37 g. For this investigation, a PGA of 0.34 g was considered, and seismic motion data was accordingly scaled. Earthquake data has been obtained from center for engineering motion data [10]. Figure 5 depicts the seismic time history, showcasing Acceleration, Velocity, and Displacement. The Acceleration seismic time history was utilised, with a prescribed displacement applied in the x-direction at the bottom of the PLAXIS model.

Regarding damping simulation, the hysteretic damping for the soil model was obtained based on the corresponding Rayleigh damping coefficients for all clay and sand layers. The Rayleigh damping equation (Eq. 5) relates the damping matrix C to a portion of the mass matrix M and a portion of the stiffness matrix K using the Rayleigh damping coefficients α and β. A 10% damping ratio was applied to the soil, while only 1% was applied to the RCC footing.

$$[c] = \alpha[M] + \beta[K] \tag{5}$$

These combined earthquake application and damping simulation procedures formed the foundation for analysing the dynamic response of the structure to seismic forces, ensuring accurate and comprehensive results for the subsequent sections of the study.

2.4 Method of calculation

In a nonlinear dynamic analysis, there are two methods of numerical integration: implicit and explicit. The UBC3D-PLM model uses the implicit integration method by default. The implicit approach is employed to solve the geometric configuration depicted in Fig. 6 in PLAXIS 3D as shown in Fig. 7. A schematic representation of a model for the current study, generated using boundary conditions in the PLAXIS program, is illustrated in Fig. 8.

## 3 Validation of the simulation analysis

The primary goal of this study was to meticulously validate observed patterns in real-world data concerning the impact of shallow foundations on liquefaction-induced phenomena within susceptible soil deposits. To achieve this, the investigation drew insights from insightful centrifuge experiments conducted by Marques et al. [26]. These pioneering tests delved into the intricate behaviour of shallow foundations on substrates encompassing both liquefiable and non-liquefiable (densified) rock layers. The results of these centrifuge experiments, retrieved from the literature, formed a pivotal reference source.

The core objective of the centrifuge tests led by Marques et al. [26] was to gain deeper insights into the seismic performance of shallow foundations constructed on liquefiable terrains, employing diverse liquefaction mitigation
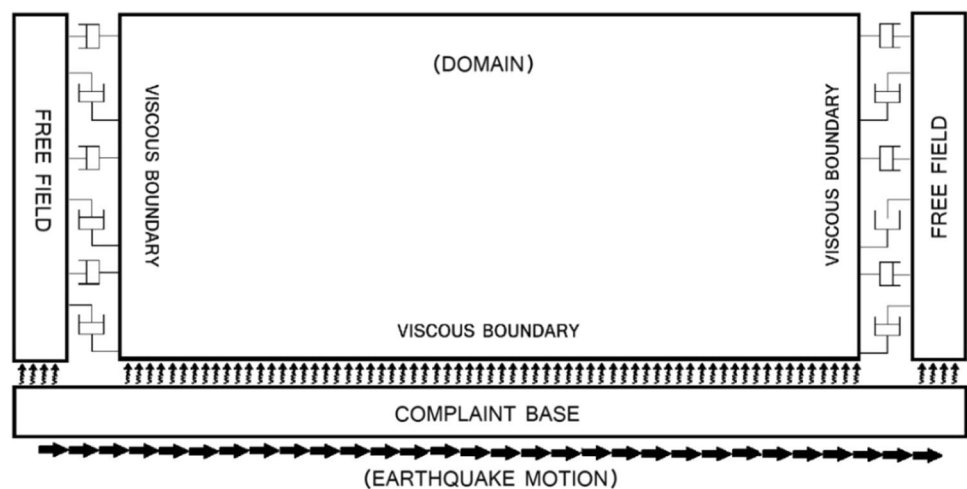
Fig. 6 Geometric diagram of soil-foundation system
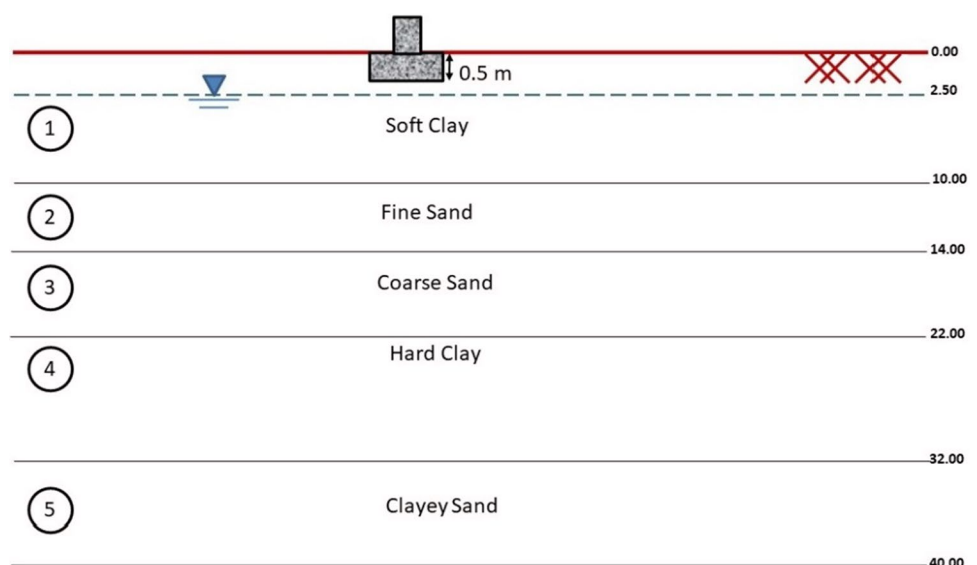
**Fig. 7** PLAXIS 3D model depicting the soil and foundation configuration
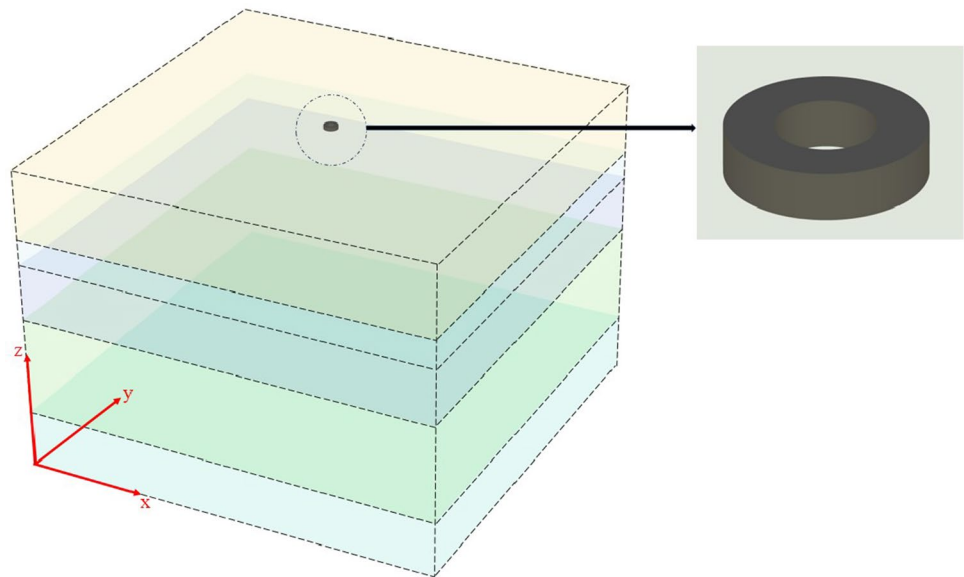
Fig. 8 A schematic representation of a present PLAXIS research problem with boundary conditions

measures. For the experimental setup, fine-grained, pristine, and uniform silica sand was utilised. Within a prototype model boasting an impressive 18-m depth, two identical shallow foundations were strategically positioned atop thin densified layers, closely resembling the thickness of the loosely packed sand layer. Notably, one of these foundations incorporated layers of vertical geotextile, significantly influencing the dynamics of the centrifuge model's response. A detailed depiction of the centrifuge model's arrangement is presented in Fig. 9.

The present study, examined the response of these shallow foundations during seismic events, specifically focusing on the development of excess pore water pressure within the surrounding soil. Figure 10, an essential visual representation, elucidates the trends in excess pore pressure at various ground levels under different footing configurations. Remarkably, during dynamic testing between the 30-s to 60-s mark, conspicuous fluctuations in excess pore water pressure emerged at varying depths. This phenomenon can be attributed to the Bhuj earthquake in 2001, which exhibited significant fluctuations in acceleration magnitude during this precise time interval.

Interestingly, the observed trends from current study closely parallel those encountered in the investigation conducted by Marques et al. [26]. In the centrifuge test, the duration of acceleration spanned approximately 35 s, during which the acceleration decreased from 0.3 g to 0 g on average. Consequently, the rate of increase in excess pore pressure notably decelerated. However, in numerical simulation of the Bhuj earthquake scenario, the seismic load endured beyond the 60-s mark, albeit with reduced acceleration. This sustained seismic influence resulted in the gradual but continuous escalation of excess pore pressure within the soil, albeit at a slower rate than before.
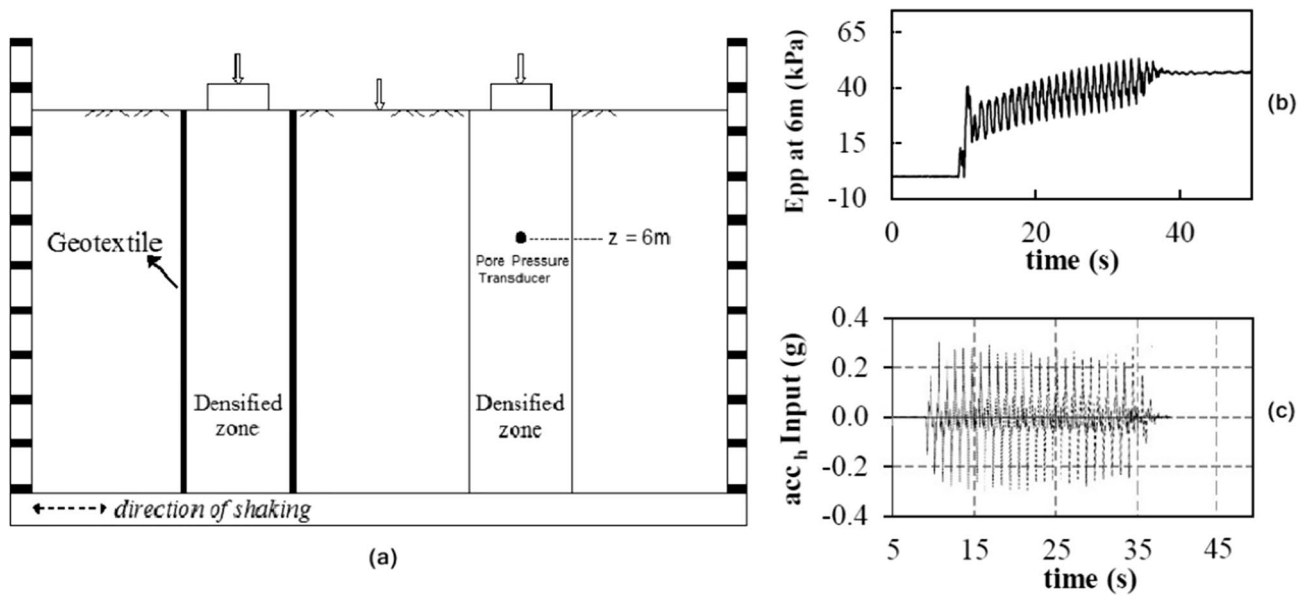
Fig. 9 **a** Layout of centrifuge test conducted; **b** Variation in Excess pore pressure at z=6 m below the footing; and **c** induced horizontal vibration force on setup [26]



Fig. 10 Excess pore water pressure–time histories in Kandla site liquefaction modelling for different ring footings at z=18 m
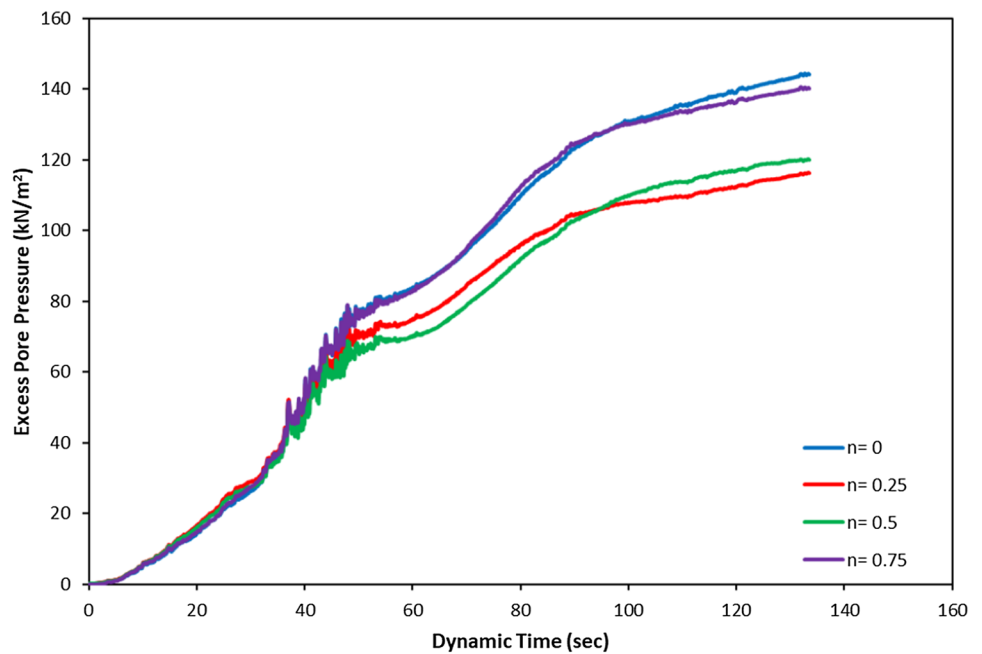
4 Result and discussion

To gain a deeper understanding of the behaviour of ring footings and circular footings in both static and dynamic conditions, computational experiments were conducted. In this study, finite element analysis using PLAXIS 3D software was employed to assess the impact of liquefaction on footings.

Fig. 11 Load-settlement curve for circular footing and ring footings resting on Kandla site soil profile
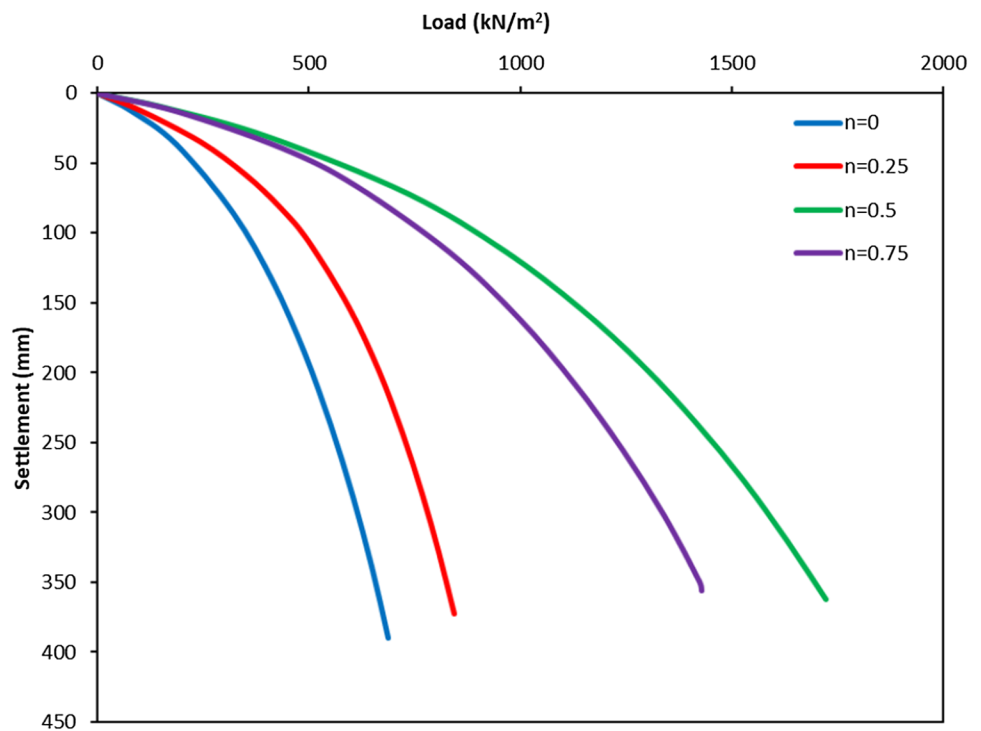
Table 5 Footing properties

Parameter	Unit	Value
Material	–	RCC (M25 grade)
Model	–	Linear elastic
Drainage type	–	Non-porous
Unit weight	kN/m^3	25
Young modulus	kN/m^2	25000000
Poisson's ratio	–	0.15

4.1 Static analysis

The outer radius (R_o) and inner radius (R_i) of the ring footing foundation are defined by the ring radius ratio, denoted as $n = (R_i/R_o)$. This investigation examined the behaviour of a solid circular footing with a radius of 1 m ($n = 0$) and three ring footings with $n = 0.25$ ($R_i = 0.25$ m), $n = 0.5$ ($R_i = 0.5$ m), and $n = 0.75$ ($R_i = 0.75$ m), while maintaining a constant outer radius ($R_o = 1$ m). Figure 11 illustrates the load-settlement variations for these different footings. It was observed that an increase in the radius ratio value (n) led to improved bearing capacity, possibly due to a reduction in the contact surface area and less constraining effect on ring footings.

Footing settlement was computed in accordance with [15]. The criteria stipulate that a reinforced concrete foundation isolated on plastic clay should not settle more than 75 mm. Table 6 displays the differences in footing settling under 100 kN/m^2 loads for various situations. Generally, the footings met the settling criteria, with solid circular footings experiencing more settlement compared to other footings. Notably, the use of ring footing with a radius ratio of $n = 0.5$ reduced settlement by over 50%, while $n = 0.25$ resulted in a reduction of over 30%. The findings for $n = 0.5$ and $n = 0.75$ were quite similar, with slightly higher settlement for $n = 0.75$. This outcome can be attributed to the fact that for a ring foundation with $n = 0.75$, there is insufficient contact surface to adequately support the foundation. Consequently, this leads to a decrease in bearing capacity, which explains why the green line is positioned to the right instead of the purple line in Fig. 11.
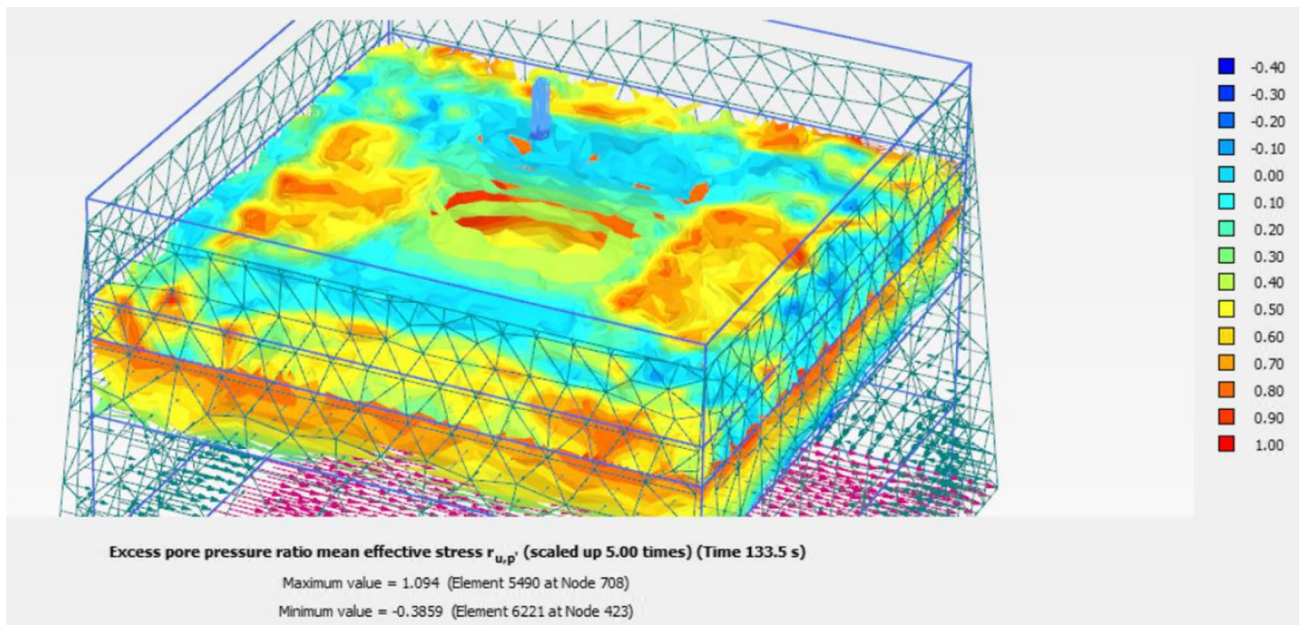
Fig. 12 Excess pore pressure ratio, r_u of sand layers under n = 0. 5 ring footing

4.2 Liquefaction analysis

The potential for liquefaction was assessed by analysing the excess pore pressure ratio (r_u), representing the ratio of excess pore pressure to initial effective vertical stress. Utilising the UBC3D-PLM model for soil behaviour, r_u was calculated using the equation:

$$r_u = 1 - \frac{\sigma'_v}{\sigma'_{v0}} \tag{6}$$

where σ'_v represents the vertical effective stress after dynamic analysis, and $\sigma'v0$ is the initial effective stress before seismic activity. When r_u equals 1, it signifies complete liquefaction in a layer. As per [3], liquefied zones are characterised by a maximum r_u exceeding 0.7. Remarkably, in our research, r_u values exceeded 1. Figure 12 reveals that for n = 0.5 ring footing, liquefaction occurred in both sand layers. The highest r_u values were 1.115, 1.237, 1.094, 1.214, and 1.090, respectively, under free field conditions, n = 0.25, 0.5, and 0.75 ring footings, and circular footings.

From numerical analysis it was observed that, ring footings and solid footings with a 0.5 m radius exhibited the lowest r_u values, indicating greater resistance to liquefaction. The findings suggest that excess pore pressure ratios beneath the footing were lower than those in the free field along the footing axis. This suggests that liquefaction beneath the foundation was challenging, possibly due to denser material settling in a soil deposit with a lower unit weight. Furthermore, it emphasises that increased distances from the footing axis, both horizontally and vertically, led to higher excess pore pressure ratios.

Liquefaction-induced settlement was studied by documenting settlement-time histories by considering vertical deformation and horizontal displacement of the footings. Figure 13 illustrates vertical footing settling under various conditions. The maximum settlement occurred under free field conditions, resulting in significant vertical distortion of the ground surface. Solid circular footings reduced vertical settlement compared to the free field, while n = 0.25 and n = 0.5 ring footings exhibited even greater reductions. The ring footing with a radius ratio of n = 0.75 had the least settling at the end of the dynamic time history. Regarding horizontal displacement (see Fig. 14), free field conditions yielded the largest horizontal displacement. Additionally, a decrease in the horizontal displacement was seen as n value increased. In contrast to previous footing examples, the outcome of ring footing with radius ratio n = 0.5 demonstrated a very high settlement.

Fig. 13 Settlement-time histories in the vertical direction
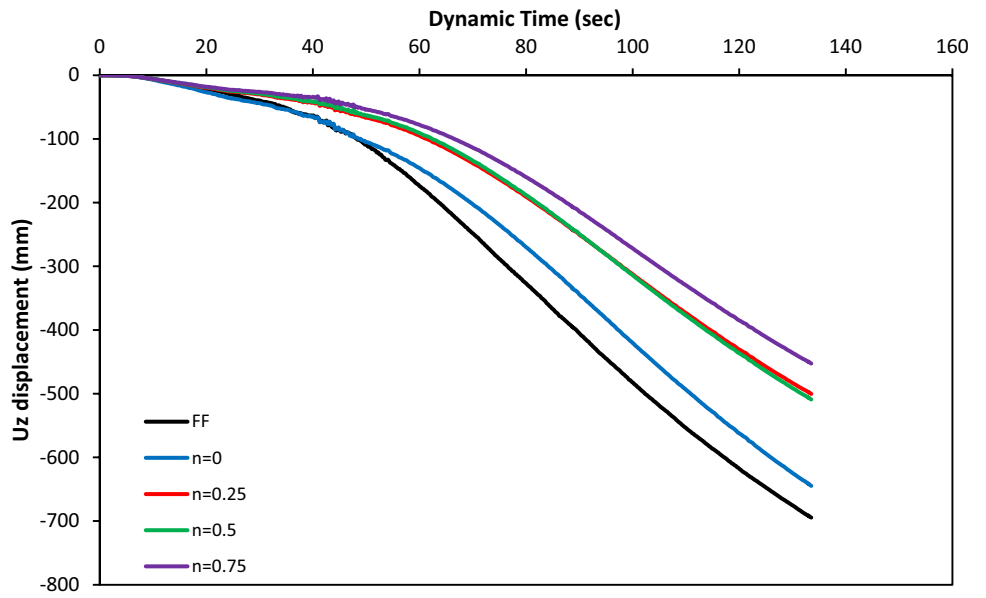
Fig. 14 Settlement-time histories in the direction of seismic force
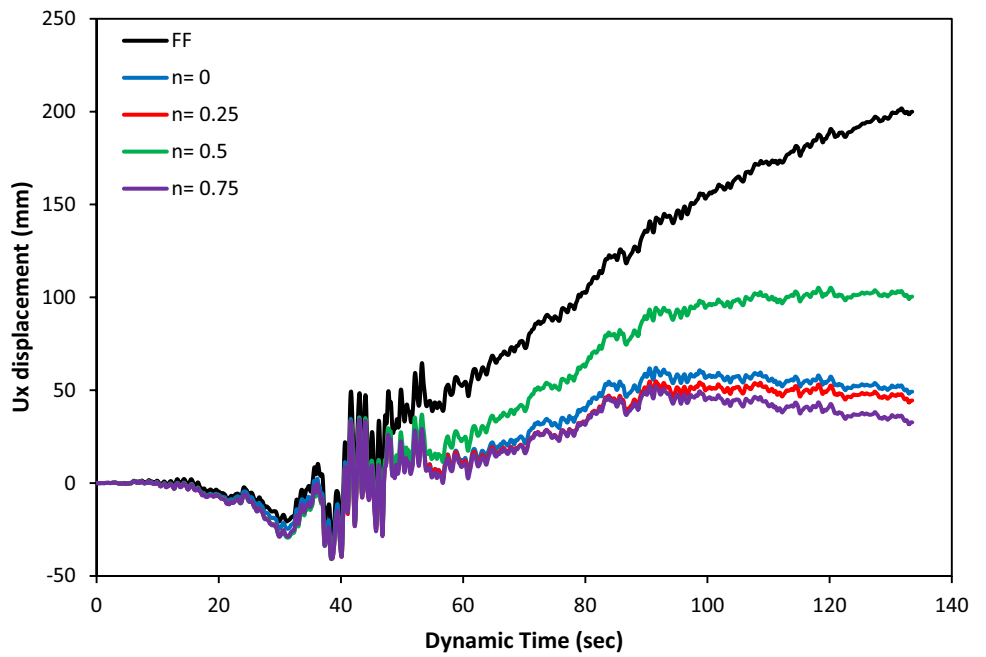
Table 6 Comparison of settlement

	n = 0	n = 0.25	n = 0.5	n = 0.75
Vertical Settlement (mm)	17.23	12.15	6.41	6.88

Table 7 Maximum mobilised friction angle in liquefying layers

	Mobilised friction angle, Φ_{mob} (°)	
	Static	Dynamic
n = 0 footing	19.84	31.87
n = 0.25 footing	19.84	31.66
n = 0.5 footing	19.85	30.79
n = 0.75 footing	19.81	30.86

4.3 Mobilised friction

The mobilisation of approximately 30° of the friction angle in a static state is essential to support the load up to the maximum bearing capacity. Notably, the type of footing had minimal influence on the mobilisation of the friction angle in this scenario. However, after subjecting the soil mass to earthquake loading, the mobilised friction angle values increased, as indicated in Table 7. These values exceeded the available soil friction angle, signifying soil collapse during an earthquake.

The effect of inner diameter of footing was evident. Furthermore, the mobilised friction angle value decreased with increasing inner diameter and transitioning from a circular to a ring footing. However, it's important to note that these changes in values were not significant enough to be considered critical. Equation 7 may be used to compute the safety factor against failure.

$$Factor\ of\ Safety = \frac{Available\ friction\ angle}{Mobilised\ friction\ angle} \tag{7}$$

In static conditions, the factor of safety exceeded 1, indicating stability. However, during an earthquake event, this value dropped below 1, demonstrating that failure occurred due to the seismic motion.

5 Conclusion

This study employed comprehensive 3D dynamic analyses using the PLAXIS 3D tool to evaluate the effects of liquefaction on shallow foundations. The investigation focused on the subsurface soil beneath the foundation, comprising layers susceptible to liquefaction, with a soft clay crust overlaying a bed of liquefiable sand. Through finite element simulation, the undrained behaviour of Kandla's wet soil strata under various ring and circular footings was effectively captured. Leveraging the earthquake time history of the 2001 $M_w = 7.7$ Bhuj, India earthquake, several crucial insights emerged that could enhance the performance of shallow foundations under seismic conditions:

1. The static ultimate bearing capacity was found to be highest for the ring footing with n = 0.5, outperforming all other ring footings and solid circular footings.
2. Notably, the ring footing with n = 0.5 exhibited the least settlement under a static load of 100kN/m², showcasing approximately a 60% reduction in settlement compared to circular footings with the same outer diameter. This underscores its practical applicability and structural resilience.
3. Dynamic analysis revealed that earthquake-induced loading resulted in liquefaction and subsequent settlement of foundations, with significantly higher settlement values observed compared to static analysis.
4. Importantly, while liquefaction was triggered in all cases, the ring footing with n = 0.5 displayed the lowest r_u value among all ring footings, ultimately leading to more favourable outcomes in terms of settlement mitigation and structural stability.

These findings underscore the importance of considering ring footing configurations, particularly those with a radius ratio of n = 0.5, in seismic design and engineering practices, offering valuable insights for enhancing the seismic resilience of shallow foundations in earthquake-prone regions. The superior performance of the ring footing with a radius ratio of n = 0.5 was anticipated prior to the modelling for several reasons. Firstly, this specific configuration strikes a balance between the inner and outer radii of the ring footing, providing optimal load distribution and foundation support.

Secondly, the selection of n = 0.5 ensures sufficient contact area with the underlying soil strata, effectively distributing the applied loads and minimising settlement.

Declarations

References

1. Beaty M, Byrne PM. An effective stress model for predicting liquefaction behavior of sand. Geotech Earthq Eng Soil Dyn. 1998;III:766–77.
2. Beaty MH, Byrne PM. UBCSAND constitutive model version 904aR. 2011.
3. Beaty MH, Perlea VG. Several observations on advanced analyses with liquefiable materials. In: 31st Annual USSD Conference and 21st Conference on Century Dam Design-Advances and Adaptations. 2011;1369–1397
4. Birid K, Choudhury D. Undrained bearing capacity factor N_c for ring foundations in cohesive soil. Int J Geomech. 2021. https://doi.org/10.1061/(ASCE)GM.1943-5622.0001900.
5. Birid K, Choudhury D. Failure envelopes for ring foundations resting on tresca soil under combined loading. J Geotech Geoenviron Eng. 2022. https://doi.org/10.1061/(ASCE)GT.1943-5606.0002900.
6. Birid K, Choudhury D. Earthquake response of ring foundation in cohesionless soil. Geotech Geol Eng. 2022;40:4269–88. https://doi.org/10.1007/s10706-022-02149-y.
7. Boushehrian J, Hataf N. Experimental and numerical investigation of the bearing capacity of model circular and ring footings on reinforced sand. Geotext Geomembr. 2003;21:241–56. https://doi.org/10.1016/S0266-1144(03)00029-3.
8. Bray JD, Dashti S. Liquefaction-induced building movements. Bull Earthq Eng. 2014;12:1129–56. https://doi.org/10.1007/s10518-014-9619-8.
9. Brinkgreve RBJ, Kumarswamy S, Swolfs WM. PLAXIS 3D Manual. Delft, Netherlands. 2015.
10. COSMOS Strong-motion program board COSMOS strong motion data format. In: COSMOS Publication
11. Dash SR, Govindaraju L, Bhattacharya S. A case study of damages of the Kandla Port and customs office tower supported on a mat–pile foundation in liquefied soils under the 2001 Bhuj earthquake. Soil Dyn Earthq Eng. 2009;29:333–46. https://doi.org/10.1016/j.soildyn.2008.03.004.
12. El Sawwaf M, Nazir A. Behavior of eccentrically loaded small-scale ring footings resting on reinforced layered soil. J Geotech Geoenviron Eng. 2012;138:376–84. https://doi.org/10.1061/(ASCE)GT.1943-5606.0000593.
13. Gass B, Ventura DFC, de Beer M. Erodibility of cemented materials. South Africa: National Department of Transport; 1993.
14. Hong Y, Lu Y, Orense RP. Effective stress simulation of liquefaction-induced building settlements. In: 16th world conference on earthquake, 16WCEE 2017. Santiago, Chil. 2017.
15. IS: 1904. Code of practice for design and construction of foundations in soils: general requirements (Third Revision). New Delhi, India. 1986.
16. IS-456. Plain and reinforced concrete—code of practice (Fourth Revision). New Delhi, India. 2000.
17. IS-1893. Indian standard criteria for earthquake resistant design of structures Part 1: general provisions and buildings (Sixth Revision). New Delhi, India. 2016.
18. IS: 6403. Code of practice for determination of bearing capacity of shallow foundations New Delhi, India. 1981.
19. Iyengar RN, Kanth STGR. Strong ground motion estimation during the Kutch, India earthquake. Pure Appl Geophys. 2006;163:153–73. https://doi.org/10.1007/s00024-005-0006-x.
20. Joyner WB, Chen ATF. Calculation of nonlinear ground response in earthquakes. Bull Seismol Soc Am. 1975;65:1315–36. https://doi.org/10.1785/BSSA0650051315.

21. Keawsawasvong S, Shiau J, Ngamkhanong C, Qui Lai V, Thongchom C. Undrained stability of ring foundations: axisymmetry, anisotropy, and nonhomogeneity. Int J Geomech. 2022. https://doi.org/10.1061/(ASCE)GM.1943-5622.0002229.

22. Keshavarz A, Kumar J. Bearing capacity computation for a ring foundation using the stress characteristics method. Comput Geotech. 2017;89:33–42. https://doi.org/10.1016/j.compgeo.2017.04.006.

23. Liyanapathirana DS, Poulos HG. A numerical model for dynamic soil liquefaction analysis. Soil Dyn Earthq Eng. 2002;22:1007–15. https://doi.org/10.1016/S0267-7261(02)00125-2.

24. Lysmer J, Kuhlemeyer RL. Finite dynamic model for infinite media. J Eng Mech Div. 1969;95:859–77. https://doi.org/10.1061/JMCEA3.0001144.

25. Makra A, Brinkgreve RBJ, Hicks MA, Bakker KJ, Witasse R. Evaluation of the UBC3D-PLM constitutive model for prediction of earthquake induced liquefaction on embankment dams. Master Thesis, Technical university in Delft. 2013.

26. Marques A, Coelho P, Cilingir U, Haigh S, Madabhushi G. Earthquake-Induced Liquefaction Effects on a Shallow Foundation. In: 15th World Conference on. Earthquake Engineering. Lisbon, Portugal. 2012. 24179–24187

27. Mehrzad B, Haddad A, Jafarian Y. Centrifuge and numerical models to investigate liquefaction-induced response of shallow foundations with different contact pressures. Int J Civil Eng. 2016;14:117–31. https://doi.org/10.1007/s40999-016-0014-5.

28. Mehrzad B, Jafarian Y, Lee CJ, Haddad AH. Centrifuge study into the effect of liquefaction extent on permanent settlement and seismic response of shallow foundations. Soils Found. 2018;58:228–40. https://doi.org/10.1016/j.sandf.2017.12.006.

29. Naeini SA, Baziar MH. Effect of fines content on steady-state strength of mixed and layered samples of a sand. Soil Dyn Earthq Eng. 2004;24:181–7. https://doi.org/10.1016/j.soildyn.2003.11.003.

30. Onur MI, Tuncan M, Tuncan A. Determination of earthquake effects on sandy soils for the city of eskisehir, turkey. Disaster Sci Eng. 2016;2:36–9.

31. Puebla H, Byrne PM, Phillips R. Analysis of CANLEX liquefaction embankments: prototype and centrifuge models. Can Geotech J. 1997;35:641–57.

32. Sargazi O, Seyedi Hosseininia E. Bearing capacity of ring footings on cohesionless soil under eccentric load. Comput Geotech. 2017;92:169–78. https://doi.org/10.1016/j.compgeo.2017.08.003.

33. Sitharam TG, Govindaraju L. Geotechnical aspects and ground response studies in Bhuj earthquake, India. Geotech Geol Eng. 2004;22:439–55. https://doi.org/10.1023/B:GEGE.0000025045.90576.d3.

34. Tokimatsu K, Hino K, Suzuki H, Ohno K, Tamura S, Suzuki Y. Liquefaction-induced settlement and tilting of buildings with shallow foundations based on field and laboratory observation. Soil Dyn Earthq Eng. 2019;124:268–79. https://doi.org/10.1016/j.soildyn.2018.04.054.

35. Tsegaye A. Plaxis liqueafaction model. Report no. 1. 2010.

36. Waheed MQ, Moutaz NA. Study simulation of shallow foundation behavior using different finite element models. J Adv Civil Eng Pract Res. 2019;8:4–9.

37. Zhou Y, Chen Y. Influence of seismic cyclic loading history on small strain shear modulus of saturated sands. Soil Dyn Earthq Eng. 2005;25:341–53. https://doi.org/10.1016/j.soildyn.2005.03.001.